inorganics

MDPI

Article

Synthesis and Structural Characterization of Potentially Topologically Non-Trivial Zintl Phases *A*CaBi (*A* = K, Rb, Cs)

Alexander Selverian and Svilen Bobev *

Department of Chemistry and Biochemistry, University of Delaware, Newark, DE 19716, USA; alexselv@udel.edu
* Correspondence: bobev@udel.edu; Tel.: +1-302-831-8720

Abstract

For the first time, the ternary Zintl phases RbCaBi and CsCaBi have been synthesized and structurally characterized via single-crystal X-ray diffraction methods. These two compounds, alongside KCaBi, are confirmed to crystallize in a tetragonal crystal system with the space group *P*4/*nmm* (no. 129) with two formula units per cell. The lattice constants increase monotonically from a = 5.3812(10) Å and c = 8.410(3) Å for KCaBi, to a = 5.4139(7) Å and c = 8.6180(17) Å for RbCaBi, and to a = 5.4709(11) Å and c = 8.914(3) Å for CsCaBi. The crystal structure can be visualized as an array of square prisms formed of Bi atoms, which are centered by alkali metal atoms, while the Ca atoms fill tetrahedra formed of Bi atoms. There are no direct Bi–Bi interactions in the crystal structure; therefore, with full cation ordering present, the chemical bonding in the *A*CaBi compounds can be rationalized within the fully ionic approximation as $A^{+}Ca^{2+}Bi^{3-}$ (*A* = K, Rb, Cs). This suggests the opening of an (narrow) energy gap between the valence and conduction bands, i.e., semiconducting behavior.

Keywords: bismuthides; crystal structure; thermoelectrics; topological insulator; single-crystal X-ray diffraction; Zintl phases

1. Introduction

Quantum materials as a whole represent a large category of materials that consist of materials like superconductors, topological materials, spin liquids, qubits, etc. Among this large group of material systems, this study focused on the field of topological materials, which in recent years have seen perhaps one of the largest expansions in interest [1–6]. Attempts to understand topological behavior predate the classification of quantum materials or even the term topological materials. The intellectual precursor of topological phases is the integer quantum Hall effect which was discovered in 1980 [7]. This effect is observed in two-dimensional electron systems that are subjected to strong magnetic fields and low temperatures, causing them to exhibit precise quantized steps in Hall resistivity, which allows for an investigation into a material's transport properties. The integer quantum Hall effect is based on Landau levels, which are essentially the eigenstates of a charge particle (an electron) moving in a uniform magnetic field in free space. A more modern view of topological phases takes into account spin–orbit coupling. When electrons with opposite spin angular momentums move in opposing directions, non-trivial electronic topology is achieved [8].

Perhaps the most common and researched type of topological material is the topological insulator. Topological insulators cannot be classified as pure insulators/semiconductors or as metals. Instead, they lie somewhere in between. Most recent research focuses on

Academic Editor: Marius Andruh

Received: 23 February 2026
Revised: 2 March 2026
Accepted: 3 March 2026
Published: 5 March 2026

three-dimensional (3D) topological insulators. These topological insulators begin to stray from the 2D model described above and must be thought of slightly differently. There are two general classes of 3D topological insulators—weak and strong—with the latter having more convoluted connection to their 2D counterparts compared to weak topological insulators. Strong topological insulators have a bulk that is insulating, but the entire surface exhibits topological surface states, i.e., it is conductive. Strong topological insulators occur when spin–orbit coupling causes inversion between the valence and conduction bands. If this band inversion occurs but the bulk remains gapped, then the material becomes a topological insulator. A key point is that through this process time-reversal symmetry is preserved, which protects the topological surface states [9]. This spin–orbit coupling, which is crucial to the formation of topological insulators, is most commonly observed in the presence of heavy metals [10]. Some examples of strong topological insulators include Bi_2Se_3 and Bi_2Te_3 [11], as well as the first experimentally realized strong 3D topological insulator $Bi_{1-x}Sb_x$ [12].

Recently, a new category of topological materials have received much interest: topological semimetals. These consist of Weyl and Dirac semimetals, which exhibit band crossing in the bulk of the material rather than just the surface, as in topological insulators. Essentially one can image Dirac semimetals through the lens of Weyl semimetals as a combination of two Weyl points with opposite chiralities. Dirac semimetals were experimentally realized, not long ago, in materials like Na_3Bi [13] and Cd_3As_2 [14].

As evident from the above, perhaps the most prominent heavy metal in many topologically relevant compounds is Bi. Often, Bi is found in a reduced state (viz. $Na_3Bi = 3 \times Na^+ + Bi^{3-}$), forming compounds known as Zintl phases. They are made from metals from groups 1 and 2 along with the more electronegative elements from groups 13 through 15. The crystal structures of these unique materials display the characteristics of both ionic-like and covalent-like bonding, satisfying the valence requirements according to the Zintl–Klemm concept [15].

Traditionally, Zintl phases have been studied as candidate materials for thermoelectric energy conversion [16,17]. More recently, they have come under renewed investigation for their potential as topological materials [2]. Density functional theory (DFT) computations, which have provided accelerated means for the exploration of yet unknown chemical compositions and structures, have also shown promise of Zintl phases as topological materials [18,19].

Our research team has had a long-standing interest in compounds of Bi within the realm of Zintl phases [20–23]. With the interest in Bi-based Zintl phases skyrocketing, we renewed our exploratory work aimed at the discovery of such new materials. Specifically, we targeted the equiatomic *AAE*Bi general compositions (*A* = alkali metal, *AE* = alkaline–earth metal), several of which have been computationally predicted to be topologically non-trivial [24–26].

In this paper, we report the synthesis and structural characterization of KCaBi, RbCaBi, and CsCaBi via single-crystal X-ray diffraction methods. The structures are new additions to the large family of compounds that are isotypic to the Cu_2Sb structure and commonly referred to as being of the anti-PbFCl structure type. In all three cases, a full cation ordering is observed, indicating that the structures obey the valence rules and the materials are expected to be semiconductors following the formula breakdown $K^+Ca^{2+}Bi^{3-}$, $Rb^+Ca^{2+}Bi^{3-}$, and $Cs^+Ca^{2+}Bi^{3-}$, i.e., they are typical Zintl phases.

2. Results

Among the structures of the three compounds presented below, only two are new; the structure of KCaBi has been previously reported [27]. We include it again in this paper since

the original determination was performed at ambient temperature, while the structures of *A*CaBi (*A* = K, Rb, Cs) discussed here are all established at 200 K. Details of data collection and selected crystallographic parameters are summarized in Table 1.

Table 1. Selected single-crystal data collection and structure refinement parameters for KCaBi, RbCaBi and CsCaBi. All three data sets were collected at 200(2) K with monochromated Mo Kα radiation, λ = 0.71073 Å.

Empirical Formula	KCaBi	RbCaBi	CsCaBi
Formula weight	288.16	334.53	381.97
Space group, Z	$P4/nmm$, 2	$P4/nmm$, 2	$P4/nmm$, 2
a (Å)	5.3812(10)	5.4139(7)	5.4709(11)
c (Å)	8.410(3)	8.6180(17)	8.914(3)
V (Å^3)	243.54(10)	252.60(7)	266.80(11)
c/a	1.562	1.592	1.629
ρ_{cal} (g/cm^3)	3.93	4.40	4.76
μ (cm^{-1})	378.9	452.8	405.3
Goodness-of-fit on F^2	1.04	1.11	1.05
Unique reflections	214	260	255
Refined parameters	10	10	10
R_1 ($I > 2\sigma_I$) [a]	0.0353	0.0301	0.0479
wR_2 ($I > 2\sigma_I$) [a]	0.0644	0.0521	0.0918
R_1 (all data) [a]	0.0425	0.0384	0.0700
wR_2 (all data) [a]	0.0661	0.0549	0.0979
Largest difference peak and hole (e^-/Å^3)	2.23 and −1.85	1.86 and −2.18	1.83 and −2.15
CCDC deposition no.	2529379	2529380	2529381

[a] $R_1 = \sum||F_o| - |F_c|| / \sum|F_o|$; $wR_2 = [\sum[w(F_o^2 - F_c^2)^2] / \sum[w(F_o^2)^2]]^{1/2}$, where $w = 1/[\sigma^2 F_o^2 + (AP)^2 + (BP)]$ and $P = (F_o^2 + 2F_c^2)/3$. A and B are the respective weight coefficients (see the CIFs).

The structure of *A*CaBi (*A* = K, Rb, Cs) is tetragonal and has the centrosymmetric space group $P4/nmm$ (no. 129). The prototype anti-PbFCl structure has been discussed in many other published works [28,29]; therefore, we will only briefly cover it. A schematic representation of the structure, drawn with thermal ellipsoids, can be found in Figure 1.

There are three independent crystallographic positions in the asymmetric unit (Table 2), including one alkali metal, one calcium, and one bismuth site, all in special positions (Pearson symbol $tP6$, Wyckoff c^2a). The structure can be described in multiple ways and related to other simpler structures, which are commonly derived from close-packed ions [30,31]. One such way of relating the *A*CaBi (*A* = K, Rb, Cs) structure to that of the ubiquitous cubic MgAgAs structure (also known as half-Heusler, a variant of the rock salt and zinc blende patterns) is depicted schematically in Figure 2. In essence, if one considers a cubic close-packed array of Bi^{3-} anions and fills the interstices with A^+ and Ca^{2+} cations as depicted in the left panel, the MgAgAs structure is realized. Such an arrangement of large ions is unlikely to be stable, and in fact, most other equiatomic *AAE*Bi compounds crystallize with different structures; only LiMgBi from the latter family is reported with the cubic MgAgAs-type structure [32]. Following a rearrangement of half of the alkali and alkaline—earth metal atoms, and subsequent unit cell expansion, the actual tetragonal PbFCl arrangement can be obtained.

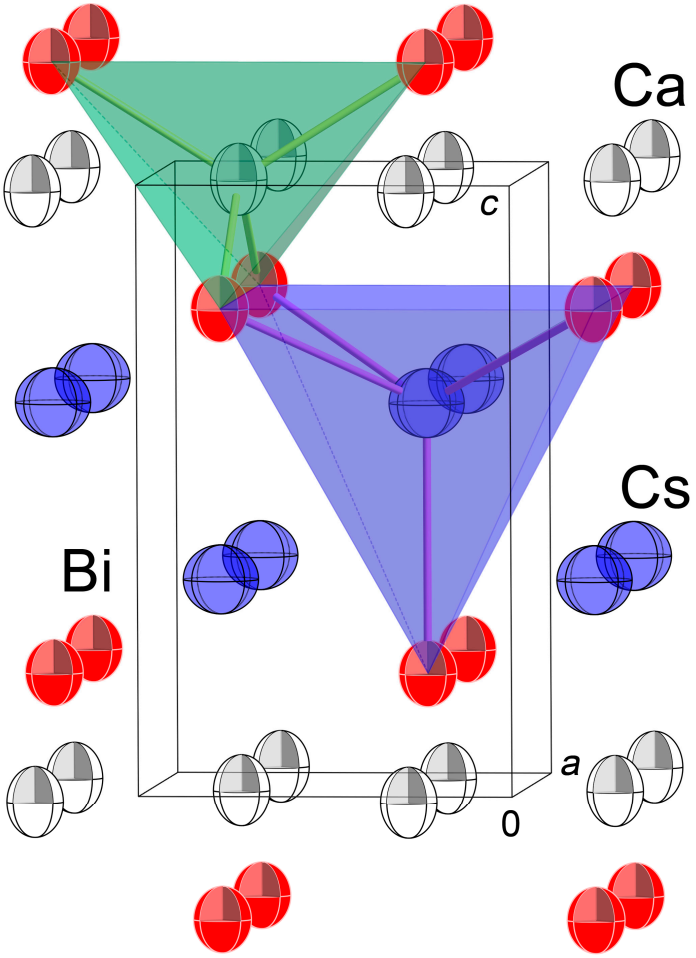

Figure 1. The tetragonal crystal structure of CsCaBi, projected approximately down the *a*-axis. The representation emphasizes the arrangement of Na-centered tetrahedra of Bi and Cs-centered square pyramids of Bi. The unit cell is outlined. Thermal ellipsoids are drawn at the 90% probability level. One should notice that U_{eq} for the *A* atoms vs. the average U_{eq} values for the Ca and Bi atoms shows a trend with U_{eq} (Cs):U_{eq} (Bi,Ca) = 1.4; U_{eq} (Rb):U_{eq} (Bi,Ca) = 2.3; and U_{eq} (K):U_{eq} (Bi,Ca) = 2.7, which could indicate that the smaller K^+ cation is not able to fit very well in the coordination environment of five Bi^{3-} anions.

Table 2. The atomic coordinates of the atoms and their equivalent isotropic displacement parameters U_{eq} [a] for KCaBi, RbCaBi and CsCaBi.

Atom	Site	*x*	*y*	*z*	U_{eq} (Å^2)
		KCaBi			
K	2*c*	1/4	1/4	0.6348(8)	0.048(2)
Ca	2*a*	3/4	1/4	0	0.019(1)
Bi	2*c*	1/4	1/4	0.2098(1)	0.0177(4)
		RbCaBi			
Rb	2*c*	1/4	1/4	0.6348(2)	0.0251(5)
Ca	2*a*	3/4	1/4	0	0.0111(7)
Bi	2*c*	1/4	1/4	0.20146(8)	0.0109(2)
		CsCaBi			
Cs	2*c*	1/4	1/4	0.6346(3)	0.0364(6)
Ca	2*a*	3/4	1/4	0	0.026(1)
Bi	2*c*	1/4	1/4	0.1924(1)	0.0251(5)

[a] U_{eq} is defined as one-third of the trace of the orthogonalized U_{ij} tensor.

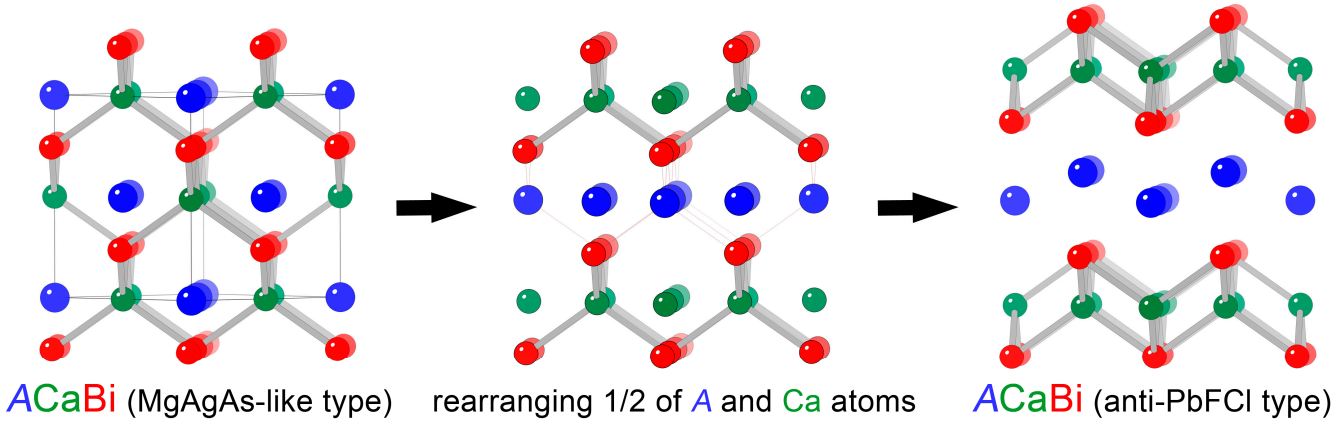

Figure 2. A schematic diagram showing how the tetragonal *A*CaBi (*A* = K, Rb, Cs) crystal structure can be derived from the cubic MgAgAs structure (close relative of the rock salt and zinc blende structures).

Another easy way of visualizing the crystal structure is as an array of square prisms of Bi atoms, centered by alkali metal atoms and Bi atom tetrahedra filled with Ca atoms, organized as shown in Figure 1. Alternating layers of prisms and tetrahedra are stacked along the *c*-direction. The much larger (relative to Ca) alkali metal atoms expand the stacking sequence, which is evident from the large increase in the *c*-axis from ca. 8.4 Å for KCaBi to ca. 8.9 Å for CsCaBi (Table 1). There also is a small elongation of the *a*-axis ongoing from KCaBi to CsCaBi, but the unit cell expansion is clearly anisotropic; the *c*/*a* ratios presented in Table 1 are a testament to that. The reason for the much smaller effect of the alkali metal on the bonding in the *ab*-plane is rooted in the fact that Ca coordination by the Bi atoms should remain nearly constant in the series. Table 3 shows selected interatomic distances, with $d_{Ca–Bi}$ varying within less that 0.5%.

Table 3. Selected interatomic distances (Å) in KCaBi, RbCaBi and CsCaBi.

Atom Pair	Distance (Å)	Atom Pair	Distance (Å)	Atom Pair	Distance (Å)
KCaBi		RbCaBi		CsCaBi	
Ca–Bi (×4)	3.2175(7)	Ca–Bi (×4)	3.2159(5)	Ca–Bi (×4)	3.2280(9)
K–Bi	3.575(7)	Rb–Bi	3.734(2)	Cs–Bi	3.943(3)
K–Bi (×4)	4.023(2)	Rb–Bi (×4)	4.0801(9)	Cs–Bi (×4)	4.165(1)

With regards to distances, it is noted that the smaller Ca atom favors "tighter" 4-fold tetrahedral coordination with $d_{Ca–Bi}$ values on the order of 3.2 Å; these are on par with the sum of the Pauling single-bonded radii of Ca (1.736 Å) and Bi (1.51 Å) [33]. At the same time, the larger alkali metal atoms are pyramidally (CN 5) coordinated but only the axial $d_{A–Bi}$ contacts come close to the sum of the Pauling single-bonded radii ($d_{K–Bi}$ = 3.57 Å vs. 2.025 + 1.51 = 3.535 Å; $d_{Rb–Bi}$ = 3.73 Å vs. 2.16 + 1.51 = 3.67 Å; $d_{Cs–Bi}$ = 3.94 Å vs. 2.35 + 1.51 = 3.86 Å). The equatorial $d_{A–Bi}$ contacts between the *A* atoms that are square–pyramidally coordinated by the Bi atoms are much longer (Table 3), indicating that these interactions might be more electrostatic than covalent in nature. The larger equivalent displacement parameters U_{eq} for K in KCaBi, Rb in RbCaBi, and Cs in CsCaBi (Table 2) are all systematically larger compared to the U_{eq} values for Ca and Bi, suggesting that the alkali metal atoms may have more "room" to move about their equilibrium positions in the referenced structures.

There are no direct Bi–Bi interactions, with the Bi atoms being over 5 Å apart from each other. Thus, *A*CaBi (*A* = K, Rb, Cs) can be thought of as salt-like $A^{+}Ca^{2+}Bi^{3-}$ compounds, i.e., a Zintl phase. Such partitioning of the valence electrons is indicative of the opening of

an (narrow) energy gap between the valence and the conduction bands, which is sought after in both thermoelectrics and topological insulators [2].

Along that line of thought, we also mention that the *A*CaBi materials could be conceptually derived from the Dirac semimetal Na_3Bi, discussed previously, the structure of which can also be rationalized as made of closed-shell Na^+ and Bi^{3-} ions. Na_3Bi crystallizes hexagonally with the centrosymmetric space group $P6_3/mmc$ (no. 194), where the majority of the Na atoms are arranged in a nearly perfect tetrahedral network with the topology of lonsdaleite [13]. The heavier alkali metals tend to form cubic A_3Bi (A = K, Rb, Cs) compounds with the full Heusler ($CuMn_2Al$) structure, which is related to the already discussed MgAgAs (Figure 2). One can then envision the substitution of two monovalent A^+ cations with one divalent AE^{2+} cation to arrive at the salt-like formulation $A^+AE^{2+}Bi^{3-}$. Also of note is the fact that in such a *gedanken* experiment, the parent A_3Bi structure would be expected to undergo substantial reconstruction to accommodate the loss of one per formula unit atom and optimize the crystal packing based on the two types of cations with differing charges and ionic sizes (Figure 2). An expansion of these ideas, taking a deeper look into the current landscape of structural data pertaining to such compounds follows in the next section.

3. Discussion

Many equiatomic *A*–*AE*–*Pn* phases (*A* = alkali metal, *AE* = alkaline–earth metal, *Pn* = pnictogen, i.e., P, As, Sb, Bi) are already known, with the first structural reports dating back over 50 years ago [32–35]. The nominally divalent Eu and Yb from the lanthanide family can also be included here since the atomic radius of Eu is close to that of Sr and the atomic radius of Yb is close to that of Ca [36]. Hence, Eu and Yb often form compounds that are isostructural to those of Sr and Ca.

If we consider all the elements (Li, Na, K, Rb, Cs; Be, Mg, Ca, Sr, Ba, Eu, Yb; P, As, Sb, Bi) that could possibly make up a ternary equiatomic *A*–*AE*–*Pn* phase, there will exist nearly 150 possible combinations. However, out of them, only 48 (roughly $^1/_3$) have been experimentally confirmed, with the corresponding structures reported in the literature (see Appendix A, where a complete list of experimentally reported *AAEPn* compounds is given). There are almost no indications that the rest of the possibilities are not synthesizable; the gaps in knowledge are likely due to the increased chemical reactivity and increased difficulty in synthesizing and analyzing the compounds with K, Rb and Cs. In fact, this article marks the first compound from this family containing Cs that has been successfully synthesized and characterized. Furthermore, modern computational approaches have predicted what the crystal structures of the many yet-to-be-discovered compounds ought to be [37–39], and it is satisfying to see partial agreement between theory and experiment with regards to CsCaBi (*vide infra*).

From the structures that are experimentally established to date, the most recurring types are schematically depicted in Figure 3. A relatively straightforward dependence on the structures with the atomic sizes has been proposed [20].

Although there is lack of experimental reports on compounds composed of the heaviest alkali metals, some prominent trends begin to emerge. For example, when A = Li, the orthorhombic TiNiSi structure (also known as MgSrSi or Co_2Si) is the dominating one. By comparison, when A = Na, the hexagonal ZrNiAl structure type is favored. The cubic MgAgAs structure type, as already mentioned, has only been observed for the composition MgLi*Pn*, which can be attributed to the smallest ionic radii of Li^+ (r = 0.59 Å) and Mg^{2+} (r = 0.57 Å) [36] compared to the rest of the alkali and alkaline–earth metals (with the exception of Be^{2+}, which is even smaller). In addition, Li^+ and Mg^{2+} are quite similar to each other and probably best suited for highly symmetric coordination by Pn^{3-} anions.

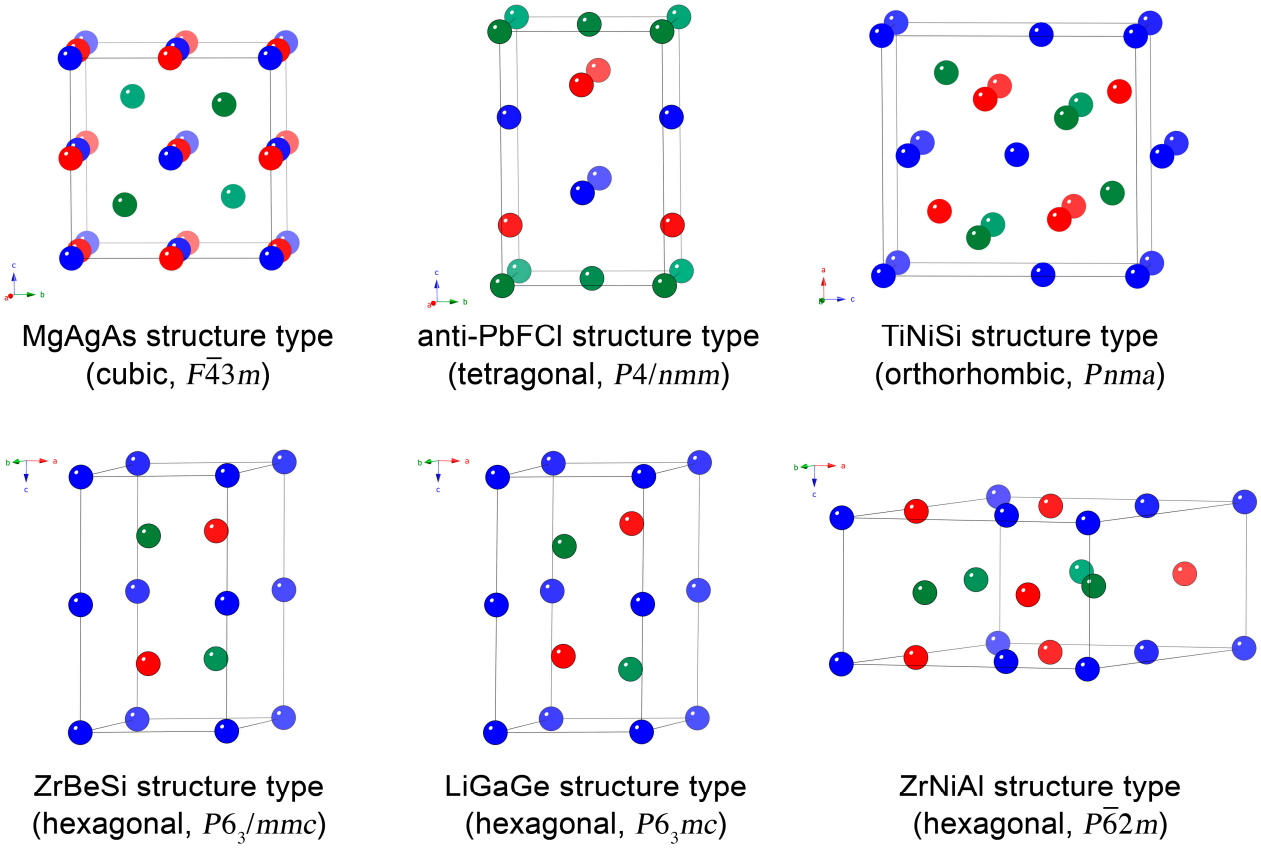

Figure 3. Schematic representations of the crystal structures of the most typical experimentally observed *A*–*AE*–*Pn* phases (*A* = alkali metal, *AE* = alkaline–earth metal, *Pn* = P, As, Sb, Bi). The *A* atoms are drawn in blue, *AE* atoms are the green spheres, and *Pn* atoms are shown in red.

When looking at other patterns in the current literature, it is observed that compounds with heavier alkali metals K and Rb tend to crystallize into the tetragonal anti-PbFCl structure type; however, it must be noted that this is the structure type with the widest range of chemical composition. The ZrBeSi structure type is largely made up of Li and Be-containing compositions. In this case, the very small Li^+ and Be^{2+} cations are able to adopt a trigonal–planar coordination environment. The LiGaGe structure is just a non-centrosymmetric variant of the ZrBeSi structure, where the 3-fold coordinated position "almost" attains a higher coordination number 4 (Figure 4). Curiously, one can envision additional structural reconstruction, whereby the structure transitions to an ordered TiNiSi-like arrangement with 4- and 5-fold coordination of the cations.

We would be remiss here if we do not mention that there are several curious cases in the published structural data which show "swapped" positions of alkali and alkaline–earth metals, or flat-out "violations" of bonding principles established from analogous compounds. One such recent exception to the rules is KBaBi, which was found to crystallize in the ZrBeSi-type structure [40]. This is the first *AAEPn* compound in the ZrBeSi structure type that contains an alkali metal heavier than Li or Na. Contrary to the trend mentioned above, Ba and K both have large atomic radii (1.981 Å and 2.025 Å, respectively) [33], making it difficult to explain the trigonal–planar coordination of Ba. This suggests that the parameters for crystallization in this structure type, and possibly other structure types too, are not understood as well as anticipated.

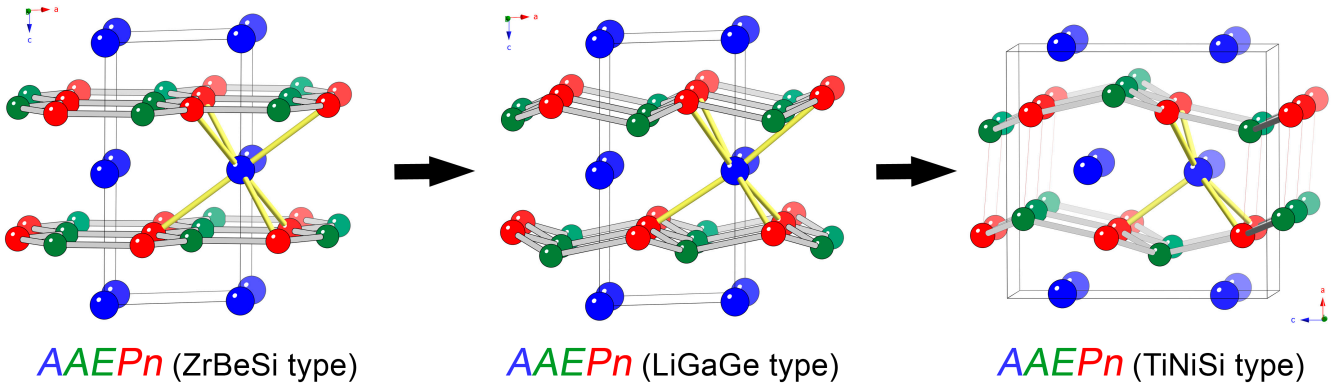

Figure 4. Schematic representations of how the *AAEPn* crystal structures of the ZrBeSi, LiGaGe, and TiNiSi types are related to each other. The honeycomb layers in the ZrBeSi-like structure (emphasized with the gray cylinders) become slightly puckered in the LiGaGe-like structure. Additional distortion allows neighboring layers to come close together and the coordination environment to become distorted tetrahedral. The coordination number of the larger cation, an alkali metal in the chosen examples, is reduced from 6 to 5 since one of the vertices of the octahedron becomes too distant.

With machine learning and various computational algorithms for structure assessment rapidly becoming mainstream approaches, one could anticipate rapid advances in this area. However, the scarcity of experimental structural information for the heavy alkali metal (Rb and Cs)-based compositions contributes to incomplete training sets, and as a result, predictive modeling may not arrive at the correct ground state structure. For example, there are predictions that RbCaBi will crystallize in the hexagonal ZrNiAl [41] as well as the ZrBeSi [25] structure types, while the experiment indicates that the correct structure is tetragonal. Similarly, CsCaBi has also been predicted to crystallize in the ZrNiAl structure by one study [41], while other models correctly identify it as being a part of the anti-PbFCl structural tree [42,43]. Clearly, further experimental investigation into all yet-to-be-synthesized compositions is warranted.

4. Materials and Methods

Maintaining inert atmosphere every step of the way is critical, because most of the complications with the synthesis and crystallographic studies arose from their extreme air and moisture sensitivity. Therefore, all synthetic and post-synthetic manipulations were carried out in an argon gas-filled glove box with O_2/H_2O levels below 1 ppm, or under vacuum (typically ca. 20 mTorr).

The synthesis procedure for KCaBi, RbCaBi and CsCaBi was adapted from the protocols used for synthesizing the previously reported Na–*AE*–*Pn* phases [44,45]. Briefly, the elements were purchased from Alfa or Sigma-Aldrich (St. Louis, MO, USA) with stated purity 99.9 wt% and used without additional purification. The elements were weighed and put in Nb tubes in the glove box. The Nb tubes were then welded shut under argon. The welded Nb tubes were subsequently placed in fused silica tubes, which were then evacuated and flame-sealed. The reactions were carried out at temperatures ranging from 600 to 800 °C (ramp rate: 300 °C/h) for 24h, and subsequently cooled to room temperature (rate −10 °C/h). Then, the tubes were put back in the glove box and cut open.

Caution: Alkali metals react quickly with air, even more so at high temperature where the reaction could be violent. Extreme care must be exercised, and to mitigate the risk, the silica jackets in such reactions should be made sufficiently long so that one of the ends of the tube protrudes outside the furnace; this is essential for the condensation of vapors in the event of a leak from the niobium ampoules into the silica tube.

X-ray powder diffraction data were collected using a Rigaku MiniFlex powder diffractometer (Rigaku Americas, The Woodlands, TX, USA), which was operated inside a nitrogen-filled glove box. Regardless of the steps taken to prevent contact of the samples with air and moisture, the X-ray powder diffraction patterns showed very high background and weak Bragg peaks, which is an indication that the samples are extremely air-sensitive and have partially decomposed in the preparation/transfer steps or during the actual experiments. The best results were obtained when the powdered samples were covered with Kapton polyimide tape. A representative powder diffraction pattern from such an experiment is shown in Figure 5.

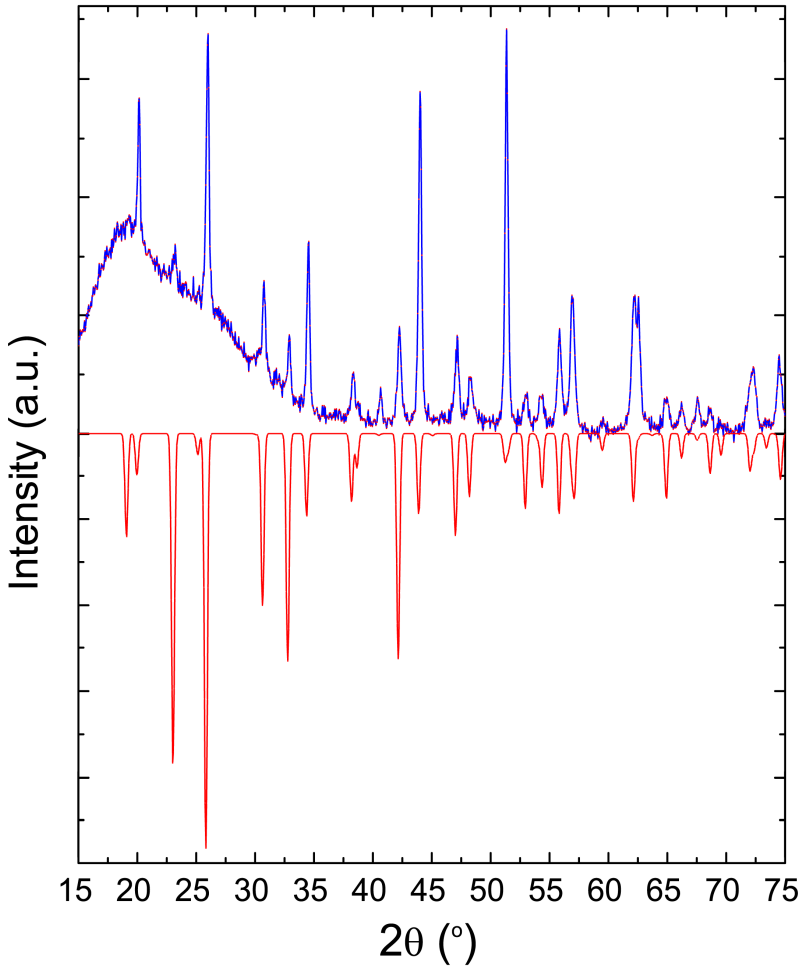

Figure 5. Experimental (blue) and simulated (red) powder diffraction patterns of CsCaBi. The high background at a low angle is contributed by the polyimide tape that protects the extremely air-sensitive material.

All additional structural characterization was performed via single-crystal X-ray diffraction. The crystals of KCaBi, RbCaBi and CsCaBi were generally small and did not have well-defined morphologies. As expected, air stability is an issue for samples with such high alkali metal contents (*vide supra*); therefore, single crystals had to be selected in the glove box. This was carried out under a microscope, with the crystals cut to dimensions of 0.10–0.20 mm. The procedure was carried out with a scalpel in a droplet of dry oil and was easily performed because the crystals were very brittle. After that, the crystals were taken out of the glove box, quickly "scooped" from the oil droplet by using MiteGen plastic loops (Ithaca, NY, USA), and transferred to the goniometer head of a Bruker APEX III CCD-based diffractometer.

For the intensity data collection, supplying nitrogen gas flow was needed to alleviate the problem of air sensitivity. Temperature was maintained at 200 K throughout the experiments via a nitrogen stream from boiled liquid N_2. The software package provided by Bruker (Madison, WI, USA) [46] was used to manage data collection and for the integration of the measured reflections. Absorption correction was applied using SADABS (version 2.03) [47]. Refinements by least-square minimizations on F^2 were carried out with the aid of the SHELXL program [48]. The atomic coordinates from the previous report on KCaBi [27] were used to create a starting model. Very reasonable conventional residual factors were obtained only after a few refinement cycles. Site occupancies were checked for each atom (for each structure) and no deviations from the unit were found. In the last refinement cycles, the atoms were refined anisotropically with SHELXL [48]. The final difference Fourier maps, in all cases, are featureless (Table 1).

5. Conclusions

Although ternary Zintl phases have been explored in the past and have provided some of the earliest topological materials, there remain large gaps in the literature as far as Zintl *AAEPn* is concerned. This is due to the increasing chemical reactivity and difficulty in synthesizing and analyzing such compounds. The lack of precise structural information and inconsistencies in knowledge are the primary reasons for the failure of some of the computational methodologies used to date to help close these gaps. Further experimental work is called for to allow for better synergy between theory and experiment and to improve the future accuracy of DFT calculations.

Author Contributions: Conceptualization, A.S. and S.B.; methodology, formal analysis, A.S. and S.B.; investigation, A.S. and S.B.; resources, S.B.; data curation, S.B.; writing—original draft preparation, S.B.; writing—review and editing, S.B.; supervision, S.B.; project administration, S.B.; funding acquisition, S.B. All authors have read and agreed to the published version of the manuscript.

Funding: This research was funded by the US Department of Energy through a grant DE-SC0008885.

Institutional Review Board Statement: Not applicable.

Informed Consent Statement: Not applicable.

Data Availability Statement: The corresponding crystallographic information files (CIFs) for all structures have been deposited with CSD, and the data for this paper can be obtained free of charge via https://www.ccdc.cam.ac.uk/structures/ (accessed on 2 March 2026) (or from the CCDC, 12 Union Road, Cambridge CB2 1 EZ, UK; Fax: +44-1223-336033; E-mail: deposit@ccdc.cam.ac.uk). Depository numbers are 2529379 (KCaBi), 2529380 (RbCaBi) and 2529381 (CsCaBi).

Acknowledgments: The authors are indebted to Salina Rahman for their help with single-crystal X-ray diffraction data collection and Daniel Tortorella for assisting with the preliminary exploratory work on *A*–*AE*–*Pn* phases.

Conflicts of Interest: The authors declare no conflicts of interest.

Abbreviations

The following abbreviations are used in this manuscript:

A	alkali metal
AE	Alkaline–earth metal
Pn	pnictogen, i.e., P, As, Sb, Bi

Appendix A

Table A1. Experimentally reported *AAEPn* compositions with their respective structure types and geometric data used to group them in the main text.

Compound	Structure Type	References
LiMgAs	MgAgAs	[32]
LiMgBi	MgAgAs	[32]
LiMgP	MgAgAs	[34,49]
LiMgSb	MgAgAs	[32]
LiCaAs	TiNiSi	[50]
LiCaBi	TiNiSi	[51]
LiCaP	TiNiSi	[52]
LiCaSb	TiNiSi	[50]
LiEuAs	TiNiSi	[50,53]
LiEuBi	TiNiSi	[50,53]
LiEuP	TiNiSi	[53]
LiEuSb	TiNiSi	[50,53]
LiSrAs	TiNiSi	[54]
LiSrBi	TiNiSi	[50,51]
LiSrSb	TiNiSi	[55]
LiYbAs	TiNiSi	[50]
LiYbBi	TiNiSi	[50]
LiYbSb	TiNiSi	[50]
LiBeSb	LiGaGe	[56]
NaBaBi	ZrNiAl	[57]
NaBaP	ZrNiAl	[58]
NaBaSb	ZrNiAl	[59]
NaEuSb	ZrNiAl	[59]
NaSrAs	ZrNiAl	[60]
NaSrP	ZrNiAl	[61]
NaSrSb	ZrNiAl	[59]
KBaBi	ZrBeSi	[40]
LiBaAs	ZrBeSi	[62]
LiBaBi	ZrBeSi	[14,20]
LiBaP	ZrBeSi	[61]
LiBaSb	ZrBeSi	[63]
LiSrP	ZrBeSi	[61]
NaBeAs	ZrBeSi	[64,65]
NaBeSb	ZrBeSi	[64,65]
CsCaBi	anti-PbFCl	This work
KCaBi	anti-PbFCl	[27]
KCaSb	anti-PbFCl	[14]
KMgAs	anti-PbFCl	[66]
KMgBi	anti-PbFCl	[64–67]
KMgP	anti-PbFCl	[66]
KMgSb	anti-PbFCl	[66]
LiBeAs	anti-PbFCl	[68]
LiBeP	anti-PbFCl	[35]
NaCaBi	anti-PbFCl	[14]
NaMgAs	anti-PbFCl	[32,45,69]
NaMgBi	anti-PbFCl	[70]
NaMgSb	anti-PbFCl	[70]
RbCaAs	anti-PbFCl	[71]
RbCaBi	anti-PbFCl	This work
RbCaSb	anti-PbFCl	[71]

References

1. Tweldebrhan, D.; Balandin, A.A. "Graphene-Like" Exfoliation of Atomically-Thin Films of Bi_2Te_3 and Related Materials: Applications in Thermoelectrics and Topological Insulators. *ECS Trans.* **2010**, *33*, 103. [CrossRef]
2. Ogunbunmi, M.O.; Bobev, S. Exploiting the fraternal twin nature of thermoelectrics and topological insulators in Zintl phases as a tool for engineering new efficient thermoelectric generators. *J. Mater. Chem. C* **2023**, *11*, 8337–8357. [CrossRef]
3. Wang, Y.; Zhu, D.; Wu, Y.; Wu, Y.; Yang, Y.; Yu, J.; Ramaswamy, R.; Mishra, R.; Shi, S.; Elyasi, M.; et al. Room temperature magnetization switching in topological insulator-ferromagnet heterostructures by spin-orbit torques. *Nat. Commun.* **2017**, *8*, 1364. [CrossRef]
4. Bandres, M.A.; Wittek, S.; Harari, G.; Parto, M.; Ren, J.; Segev, M.; Christodoulides, D.M.; Khajavikhan, M. Topological insulator laser: Experiments. *Science* **2018**, *359*, eaar4005. [CrossRef] [PubMed]
5. Pesin, D.; MacDonald, A. Spintronics and pseudospintronics in graphene and topological insulators. *Nat. Mater.* **2012**, *11*, 409–416. [CrossRef] [PubMed]
6. Rajamathi, C.R.; Gupta, U.; Kumar, N.; Yang, H.; Sun, Y.; Süß, V.; Shekhar, C.; Schmidt, M.; Blumtritt, H.; Werner, P.; et al. Weyl Semimetals as Hydrogen Evolution Catalysts. *Adv. Mater.* **2017**, *29*, 1606202. [CrossRef]
7. Klitzing, K.V.; Dorda, G.; Pepper, M. New Method for High-Accuracy Determination of the Fine-Structure Constant Based on Quantized Hall Resistance. *Phys. Rev. Lett.* **1980**, *45*, 494. [CrossRef]
8. Murakami, S.; Nagaosa, N.; Zhang, S. Spin-Hall Insulator. *Phys. Rev. Lett.* **2004**, *93*, 156804. [CrossRef] [PubMed]
9. Moore, J.E.; Balents, L. Topological invariants of time-reversal-invariant band structures. *Phys. Rev. B* **2007**, *75*, 121306(R). [CrossRef]
10. Xia, Y.; Qian, D.; Hsieh, D.; Wray, L.A.; Pal, A.; Lin, H.; Bansil, A.; Grauer, D.C.; Hor, Y.S.; Cava, R.J.; et al. Observation of a large-gap topological-insulator class with a single Dirac cone on the surface. *Nat. Phys.* **2009**, *5*, 398–402. [CrossRef]
11. Zhang, H.; Liu, C.X.; Qi, X.L.; Dai, X.; Fang, Z.; Zhang, S. Topological insulators in Bi_2Se_3, Bi_2Te_3 and Sb_2Te_3 with a single Dirac cone on the surface. *Nat. Phys.* **2009**, *5*, 438–442. [CrossRef]
12. Hsieh, D.; Qian, D.; Wray, L.; Xia, Y.; Hor, Y.S.; Cava, R.J.; Hasan, M.Z. A topological Dirac insulator in a quantum spin Hall phase. *Nature* **2008**, *452*, 970–974. [CrossRef] [PubMed]
13. Liu, Z.K.; Zhou, B.; Wang, Z.J.; Weng, H.M.; Prabhakaran, D.; Mo, S.K.; Zhang, Y.; Shen, Z.X.; Fang, Z.; Dai, X.; et al. Discovery of a Three-Dimensional Topological Dirac Semimetal, Na_3Bi. *Science* **2014**, *343*, 864–867. [CrossRef]
14. Neupane, M.; Xu, S.Y.; Sankar, R.; Alidoust, N.; Bian, G.; Liu, C.; Belopolski, I.; Chang, T.; Jeng, H.; Lin, H.; et al. Observation of a three-dimensional topological Dirac semimetal phase in high-mobility Cd_3As_2. *Nat. Commun.* **2014**, *5*, 3786. [CrossRef]
15. Miller, G.J.; Schmidt, M.W.; Wang, F.; You, T.-S. Quantitative Advances in the Zintl-Klemm Formalism. In *Zintl Phases: Principles and Recent Developments*; Fassler, T.F., Ed.; Structure and Bonding; Springer: Berlin/Heidelberg, Germany, 2011; Volume 139, pp. 1–55.
16. Wang, Z.; Sun, Y.; Chen, X.; Franchini, C.; Xu, G.; Weng, H.; Dai, X.; Fang, W. Dirac semimetal and topological phase transitions in A_3Bi (A = Na, K, Rb). *Phys. Rev. B* **2012**, *85*, 195320. [CrossRef]
17. Brown, S.R.; Kauzlarich, S.M.; Gascoin, F.; Snyder, G.J. $Yb_{14}MnSb_{11}$: New High Efficiency Thermoelectric Material for Power Generation. *Chem. Mater.* **2006**, *18*, 1873–1877. [CrossRef]
18. Zhu, Z.; Li, M.; Li, J. Topological semimetal to insulator quantum phase transition in the Zintl compounds Ba_2X (X = Si, Ge). *Phys. Rev. B* **2016**, *94*, 155121. [CrossRef]
19. Feng, L.; Villaos, R.A.B.; Maghirang, A.B., III; Huang, Z.; Hsu, C.; Lin, H.; Chuang, F. Prediction of topological Dirac semimetal in Ca-based Zintl layered compounds CaM_2X_2 (M = Zn or Cd; X = N, P, As, Sb, or Bi). *Sci. Rep.* **2022**, *12*, 4582. [CrossRef] [PubMed]
20. Ovchinnikov, A.; Bobev, S. Crystal and electronic structure of the ternary Zintl bismuthide BaLiBi. *Z. Anorg. Allg. Chem.* **2023**, *649*, e202300128. [CrossRef]
21. Janzen, R.; Baranets, S.; Bobev, S. Synthesis and structural characterization of the new Zintl phases $Eu_{10}Mn_6Bi_{12}$ and $Yb_{10}Zn_6Sb_{12}$. *Dalton Trans.* **2022**, *51*, 13470–13478. [CrossRef]
22. Baranets, S.; Bobev, S. Caught in Action. The Late Rare Earths Thulium and Lutetium Substituting Aluminum Atoms in the Structure of $Ca_{14}AlBi_{11}$. *J. Am. Chem. Soc.* **2021**, *143*, 65–68. [CrossRef] [PubMed]
23. Baranets, S.; Bobev, S. $Ca_{14}AlBi_{11}$—A new Zintl phase from earth-abundant elements with a great potential for thermoelectric energy conversion. *Mater. Today Adv.* **2020**, *7*, 100094. [CrossRef]
24. Patel, S.; Patel, P.; Dhori, B.R.; Jha, P.K. Topological Phase Transition in Non-centrosymmetric LiCaBi Compound: A First-principles Study. *J. Phys. Chem. C* **2024**, *128*, 7766–7772. [CrossRef]
25. Zhang, X.; Liu, Q.; Xu, Q.; Dai, X.; Zunger, A. Topological Insulators versus Topological Dirac Semimetals in Honeycomb Compounds. *J. Am. Chem. Soc.* **2018**, *140*, 13687–13694. [CrossRef] [PubMed]
26. Shao, D.; Gua, Z.; Wu, X.; Nie, S.; Sun, J.; Weng, H.; Wang, Z. Topological insulators in the NaCaBi family with large spin-orbit coupling gaps. *Phys. Rev. Res.* **2021**, *3*, 013278. [CrossRef]
27. Hirt, H.; Deiseroth, H.J. Crystal structure of potassium calcium bismuthide, KCaBi. *Z. Kristallogr.* **2003**, *218*, 5.

28. Nica, E.M.; Yu, R.; Si, Q. Glide reflection symmetry, Brillouin zone folding, and superconducting pairing for the P4/*nmm* space group. *Phys. Rev. B* **2015**, *92*, 174520. [CrossRef]
29. Eisenmann, B.; Schäfer, H.; Weiss, A. Der Übergang vom "geordneten" Anti-$PbCl_2$-Gitter zum Anti-PbFCl-Gitter: Ternäre Phasen ABX der Erdalkalimetalle mit Elementen der 4. Hauptgruppe (A = Ca, Sr, Ba; B = Mg; X = Si, Ge, Sn, Pb). *Z. Anorg. Allg. Chem.* **1972**, *391*, 241–264. [CrossRef]
30. Nuss, J.; Jansen, M. Zur Abgrenzung der PbFCl- und Cu_2Sb-Strukturfamilien: Neubestimmung und Verfeinerung der Kristallstrukturen von CuMgSb, Cu_2Sb und CuMgAs. *Z. Anorg. Allg. Chem.* **2002**, *628*, 1152–1157. [CrossRef]
31. Nuss, J.; Wedig, U.; Jansen, M. Geometric variations and electron localizations in intermetallics: PbFCl type compounds. *Z. Kristallogr.* **2009**, *221*, 554–562. [CrossRef]
32. Nowotny, H.; Holub, F. Untersuchungen an metallischen Systemen mit Flußspatphasen. *Monatsh. Chem.* **1960**, *91*, 877–887. [CrossRef]
33. Pauling, L. Atomic Radii and Interatomic Distances in Metals. *J. Am. Chem. Soc.* **1947**, *69*, 542–553. [CrossRef]
34. Nowotny, H.; Bachmayer, K. Die Verbindungen LiMgP, LiZnP und LiZnAs. *Monatsh. Chem.* **1949**, *80*, 734. [CrossRef]
35. El Maslout, A.; Motte, J.P.; Courtois, A.; Gleitzer, C. Phosphures ternaires de lithium. II. Structure cristalline de LiBeP. *J. Solid State Chem.* **1975**, *15*, 213–217. [CrossRef]
36. Baranets, S.; Ovchinnikov, A.; Bobev, S. *Handbook on the Physics and Chemistry of Rare Earths*; Bünzli, J.-C.G., Pecharsky, V.K., Eds.; Elsevier: Amsterdam, The Netherlands, 2021; pp. 227–324.
37. Zhang, X.; Yu, L.; Zakutyev, A.; Zunger, A. Sorting Stable versus Unstable hypothetical Compounds: The Case of Multi-Functional ABX Half-Heusler Filled Tetrahedral Structures. *Adv. Funct. Mater.* **2012**, *22*, 1425–1435. [CrossRef]
38. Sun, Y.; Wang, Q.; Wu, S.; Felser, C.; Liu, C.; Yan, B. Pressure-induced topological insulator in NaBaBi with right-handed surface spin texture. *Phys. Rev. B* **2016**, *93*, 205303. [CrossRef]
39. Sanjeev; Singh, M.; Kumar, R.; Srivastava, S.; Kumar, T. Structural, electronic and topological properties of NaCaBi and KBaBi compounds. *J. Phys. Chem. Solids* **2022**, *161*, 110416. [CrossRef]
40. Yamada, T.; Ohji, J.; Hosono, A. Investigation of a Ternary Zintl Phase KBaBi: Synthesis, Crystal Structure, and Preliminary Transport Properties. *Z. Anorg. Allg. Chem.* **2025**, *651*, e202500064. [CrossRef]
41. Mondal, C.; Barman, C.K.; Kumar, S.; Alam, A.; Pathak, B. Emergence of Topological insulator and Nodal line semi-metal states in XX′Bi (X = Na, K, Rb, Cs; X′ = Ca, Sr). *Sci. Rep.* **2019**, *9*, 527. [CrossRef]
42. Wang, H.C.; Botti, S.; Marques, M.A.L. Predicting stable crystalline compounds using chemical similarity. *npj Comput. Mater.* **2021**, *7*, 12. [CrossRef]
43. Liang, Y.; Zhao, Y.; Wang, X.; Ni, J.; Dai, Z. Rattling-driven low thermal conductivity in CsCaX (X = Bi, P) and anomalous optical phonon dominance in CsCaP. *Phys. Rev.* **2025**, *24*, 034028. [CrossRef]
44. Hirt, H. Umsetzung von Kaliumamalgamen mit Oxiden Sowie Beiträge zur Festkörperchemie Binärer und Ternärer Pniktide aus Metallen der Ersten und Zweiten Gruppe. Ph.D. Thesis, Universität Siegen, Siegen, Germany, 2004.
45. Yamada, T.; Matsuo, N.; Enoki, M.; Yamane, H. A novel ternary bismuthide, NaMgBi: Crystal and electronic structure and electrical properties. *Z. Naturforsch. B* **2021**, *76*, 789–795. [CrossRef]
46. *SAINT*, version 2.03; Bruker AXS Inc.: Madison, WI, USA, 2014.
47. *SADABS*, version 2.03; Bruker AXS Inc.: Madison, WI, USA, 2014.
48. Sheldrick, G.M. Crystal structure refinement with SHELXL. *Acta Crystallogr. C* **2015**, *71*, 3–8. [CrossRef]
49. El Maslout, A.; Motte, J.P.; Gleitzer, C.; Aubry, J. Preparation et proprietes d'un nouveau compose dans la serie LiMP: Le phosphure de lithium-cadmium LiCdP. *Comptes Rendus Seances L'academie Sci. Ser. C Sci. Chim.* **1971**, *273*, 707–710.
50. Schäfer, M.C.; Suen, N.-T.; Bobev, S. Synthesis and crystal chemistry of new ternary pnictides containing lithium—Adding structural complexity one step at a time. *Dalton Trans.* **2014**, *44*, 16889–16901. [CrossRef] [PubMed]
51. Eisenmann, B.; Schäfer, H.; Turban, K. Neue intermetallische Verbindungen im anti-$PbCl_2$ Typ. *Z. Naturforsch. B* **1975**, *30*, 677–680. [CrossRef]
52. Albering, J.H.; Ebel, T.; Jeitschko, W. Kristallstruktur und magnetische Eigenschaften der Verbindungen LiAX (A = Ca, Sr, Ba, Eu, Yb; X = P, As, Sb, Bi). *Z. Kristallogr.* **1997**, *12*, 242.
53. Prill, M.; Mosel, B.D.; Müller-Warmuth, W.; Albering, J.; Ebel, T.h.; Jeitschko, W. Mössbauer studies and magnetic properties of the novel ternary europium pnictides LiEuPn (Pn = P, As, Sb, Bi) with TiNiSi type structure. *Solid State Sci.* **2002**, *4*, 695–700. [CrossRef]
54. Feng, Z.-J.; Prots, Y.; Schmidt, M.P.; Hoffmann, S.; Veremchuk, I.; Schnelle, W.; Burkhardt, U.; Zhao, J.-T.; Grin, Y. Synthesis, structure, and properties of two Zintl phases around the composition SrLiAs. *Inorg. Chem.* **2013**, *52*, 8971–8978. [CrossRef]
55. Gupta, S.; Ganguli, A. Synthesis, structure and properties of a new Zintl phase: SrLiSb. *J. Solid State Chem.* **2006**, *179*, 1318–1322. [CrossRef]
56. Tiburtius, C.; Schuster, H.-U. LiBeSb und LiZnBi, ternaere Verbindungen mit Wurtzitgeruest. *Z. Naturforsch. B* **1978**, *33*, 35–38. [CrossRef]

57. Hirt, H.; Deiseroth, H.-J. The New Polar Intermetallic Compound NaBaBi. *Z. Anorg. Allg. Chem.* **2004**, *630*, 1357–1359. [CrossRef]
58. Carrillo-Cabrera, W.; Somer, M.; Peters, E.-M.; Peters, K.; von Schnering, H.-G. Crystal Structure of Sodium Barium Phosphide, NaBaP. *Z. Kristallogr.* **1996**, *211*, 191. [CrossRef]
59. Wang, Y.; Bobev, S. Synthesis and Crystal Structure of the Zintl Phases NaSrSb, NaBaSb and NaEuSb. *Materials* **2023**, *16*, 1428. [CrossRef]
60. Carrillo-Cabrera, W.; Somer, M.; Peters, E.-M.; Peters, K.; von Schnering, H.-G. Crystal structure of sodium strontium arsenide, NaSrAs. *Z. Kristallogr.* **1997**, *212*, 52. [CrossRef]
61. Dong, Y.; DiSalvo, F.J. Synthesis and single crystal structures of ternary phosphides Li_4SrP_2 and AAeP (A = Li, Na; Ae = Sr, Ba). *J. Solid State Chem.* **2007**, *180*, 432–439. [CrossRef]
62. The Open Quantum Materials Database. Available online: https://oqmd.org (accessed on 16 February 2026).
63. Monconduit, L.; Belin, C. A new ternary antimonide phase, LiBaSb. *Acta Crystallogr. E* **2001**, *57*, i17–i18. [CrossRef]
64. Tiburtius, C.; Schuster, H.-U. Na Be As (Sb)—Ternaere Phasen im 'aufgefuellten' Ni As (Ni_2In)-Typ. *Z. Naturforsch. B* **1977**, *32*, 1133–1138. [CrossRef]
65. Cai, Y.; Faizan, M.; Shen, X.; Mebed, A.M.; Alrebdi, T.A.; He, X. NaBeAs and NaBeSb: Novel Ternary Pnictides with Enhanced Thermoelectric Performance. *J. Phys. Chem. C* **2023**, *127*, 1733–1743. [CrossRef]
66. Vogel, R.; Schuster, H.-U. Neue elektrovalente ternäre Verbindungen des Kaliums mit Magnesium und Elementen der 5. Hauptgruppe. *Z. Naturforsch. B* **1979**, *34*, 1719–1721. [CrossRef]
67. Zhang, X.; Sun, S.; Lei, H. Narrow-gap semiconducting properties of KMgBi with multiband feature. *Phys. Rev. B* **2017**, *95*, 035209. [CrossRef]
68. Schuster, H.-U.; Tiburtius, C. Notizen: Ternäre Verbindungen in den Dreistoffsystemen Lithium(Natrium)-Beryllium-Arsen./Ternary Compounds in the System Lithium(Sodium)-Beryllium-Arsenic. *Z. Naturforsch. B* **1976**, *31*, 1536–1537. [CrossRef]
69. Krenkel, B.; Schuster, H.-U. Crystal structure of potassium calcium bismuthide, KCaBi. *Z. Naturforsch. B* **1978**, *33*, 1080–1082. [CrossRef]
70. Somer, M.; Carrillo-Cabrera, W.; Peters, E.-M.; Peters, K.; von Schnering, H.-G. NaMgAs(Sb)—Ternaere Verbindungen mit modifizierter Cu_2Sb-Struktur. *Z. Kristallogr.–Cryst. Mater.* **1996**, *211*, 633. [CrossRef]
71. Gil, R.H.C.; Caroca-Canales, N.; Hönle, W.; von Schnering, H.-G. Crystal structures of rubidium calcium arsenide, RbCaAs and of rubidium calcium antimonide, RbCaSb. *Z. Kristallogr.–New Cryst. Struct.* **1998**, *213*, 483–484.